Surface Analysis and *In Vitro* Corrosion Properties in Artificial Saliva of Surface-Treated Ti6Al4V Alloy for Dental Applications

M.A. HUSSEIN, A. MADHAN KUMAR, AHMED F. ABDELAAL, and M. ABDUL AZEEM

Ti alloys are commonly used in dental applications. The surface properties of the implants influence *in vitro* corrosion, protein adhesion, and osseointegration. The objective of this work was to investigate the influence of surface modification: plasma treatment, sandblasting, and acid treatment on the surface roughness, wettability, surface energy, and electrochemical corrosion properties in artificial saliva of Ti6Al4V alloy for dental applications. Surface analysis was carried out using AFM, optical profilometry, XRD, SEM/EDX, and contact angle measurements. *In vitro* corrosion resistance analyses of surface-treated Ti6Al4V substrates were performed in artificial saliva (AS) with and without fluorides. The surface analysis results showed that sandblasting decreased the crystallite size of the alloy surface to 10.8 nm. The hydrophilicity was improved through plasma treatment and sandblasting, as evidenced by the decrease in the water contact angle to 15 and 35 deg, respectively. The surface energy, after plasma treatment and sandblasting, increased by 10 and 28 pct, respectively. The *in vitro* corrosion test results validated the effective role of different surface treatments on the corrosion resistance behavior of Ti6Al4V substrates in AS medium with and without fluorides. The results showed that the treated Ti6Al4V alloy had improved surface and biocorrosion properties, making it a potential candidate for dental applications.

I. INTRODUCTION

TI and Ti alloys have shown higher resistance to corrosion, biocompatibility, and lower elasticity and formability than Co-based alloys and stainless steel.[1] Therefore, they are widely applied in the biomedical field,[2] especially in orthopedic and dental applications.[3,4] The surface properties of the implants, such as roughness, wettability, and surface energy affect the corrosion properties, cell adhesion, protein adhesion, proliferation,[5] and the lifetime of the implant.[6] Surface treatment is used for dental implants to modify the surface morphology and energy, resulting in better wettability,[7] increased cell proliferation, and enhanced osseointegration.[8] Commercial Ti6Al4V (Ti64) alloys have been used in orthopedic and dental applications.[9] Several surface treatment techniques have been reported using chemical,[10,11] polishing,[12] SLA,[13] and laser treatments.[14,15] The corrosion performance of the implant surface is affected by the different surface treatments. The physiological environment is aggressive and contains proteins, amino acids, and organic compounds. Implant corrosion causes the release of metal ions, which can impact the implant's biocompatibility.[16] In addition, the rate of corrosion in the oral environment is high owing to the presence of fluoride ions.[17] Ti and Ti alloys are more corrosive resistant owing to the spontaneous formation of a surface layer of native oxides. However, damage to the oxide layer due to mechanical or chemical factors affects the corrosion properties of Ti alloys. Several surface treatment methods have been proposed to modify the surface morphology, enhance the corrosion resistance of Ti alloys, and reduce metal ion release. Surface characteristics are a key factor in the corrosion and tribocorrosion behavior of Ti alloys.[18] A previous study reported the corrosion properties of untreated Ti64 alloy,[19] surface finished effect in physiological solution,[20] and surface

M.A. HUSSEIN is with the Interdisciplinary Research Center for Advanced Materials, King Fahd University of Petroleum & Minerals (KFUPM), Dhahran 31261, Saudi Arabia. Contact e-mails: mahussein@kfupm.edu.sa; mahussein1980@gmail.com A. MADHAN KUMAR is with the Interdisciplinary Research Center for Advanced Materials, King Fahd University of Petroleum & Minerals (KFUPM). AHMED F. ABDELAAL and M. ABDUL AZEEM are with the Department of Mechanical Engineering, King Fahd University of Petroleum & Minerals (KFUPM), Dhahran 31261, Saudi Arabia.
Manuscript submitted April 27, 2021; accepted July 4, 2021.
Article published online July 16, 2021.

treatment influence of Ti64 alloy in Hank's solution.[21] A limited study reported the effect of the surface treatment of Ti64 alloy on the *in vitro* corrosion performance in an artificial saliva (AS) medium. Thus, this study aims to evaluate the influence of three different surface treatment processes on the surface characteristics and *in vitro* corrosion performance of Ti64 alloys for dental applications. The surface characteristics were investigated in terms of microstructure, surface roughness, wettability, and surface energy using various analytical tools: XRD, SEM/EDX, AFM, surface profilometry, and contact angle measurements (CA). *In vitro* corrosion studies were conducted in an AS medium.

II. EXPERIMENTAL WORK

A. Material and Sample Preparation

A commercial Ti64 alloy with a size of $20 \times 20 \times 3$ mm^3 was purchased from Xian Saite Materials Development Co., China. The samples were ground using 200, 400, and 600 SiC, polished with a 0.5 μm Al_2O_3 solution, and washed with water followed by ethanol.

B. Surface Treatments

The polished Ti64 alloy was treated using three different methods: sandblasting (SB), chemical treatment (CT), and plasma treatment (PT). Sandblasting was performed using a TRINCOTM Dry Blast Machine (Model 30 Suction Blast Cabinet) with a pressure of 0.55 MPa and an air flow of 0.45 m^3/min. The distance between the nozzle and the samples remained constant for all samples, and the orientation angle of the nozzle was ~ 75 deg. The sandblasting operation lasted for 5 minutes. Chemical treatment was performed using a chemical mixture of sulfuric acid (H2SO4) (95.0 to 98.0 pct, Fisher Chemical TM), hydrochloric acid (HCl) (36.5 to 38.0 pct, Fisher Chemical TM), and deionized (DI) water with a volume percentage of 3:3:9, respectively, to treat the substrate surface at an ambient temperature for 20 minutes. The plasma cleaner model PDC-32G, manufactured by Harrick Plasma, was used for the air plasma treatment for 20 min.

C. Structure and Microstructure Characterization

XRD (Rigaku, Kuraray, Japan) with Cu Kα radiation with a wavelength of 0.15406 nm, conducted at 40 kV and 30 mA, was used for the analysis of the phases. The 2θ angle was varied between 20 and 90 deg at a step size of 0.02 deg and scanning rate of 1.2 deg/min. The surface morphologies of the untreated and treated Ti64 alloys were analyzed using field emission scanning electron microscopy (FESEM) (FEI Quanta 250). The elemental composition of the coatings was analyzed using EDX (Oxford).

D. Surface Morphology and Roughness Measurements

GTK-A, a 3D optical profiler from Bruker Co., was used to characterize the surface roughness. At least five measurements were performed, each at a different location. The topography and surface roughness of the Ti64 alloy before and after surface treatment were characterized using AFM (Agilent 5500).

E. Wettability and Surface Energy

The wetting behavior of the samples was analyzed using contact angle measurements under the sessile drop method using an optical contact angle measurement goniometer (DM-501, Kyowa Interface Science Co. Ltd, Japan). For each measurement, at least five measurements were taken using water and glycerol (3 μL), and the mean value was reported. The surface energy was calculated based on Owens-Wendt.[14,22,23]

F. In Vitro Corrosion Study in Artificial Saliva

The *in vitro* corrosion resistance behavior of the surface-treated Ti64 alloy substrates was examined using a Gamry Reference 3000 potentiostat connected to a three-cell electrode assembly. The testing medium, AS solution, was prepared by adopting a procedure based on a previous report.[14] To evaluate the influence of fluoride on the corrosion resistance of the treated Ti64 alloy substrates, 1000 ppm of NaF was added to the AS solution during the electrochemical corrosion test. The working electrode was a Ti64 alloy substrate with an exposure area of 0.2 cm^2, and a graphite rod and saturated calomel electrode (SCE) were used as the auxiliary and reference electrodes, respectively. The potentiodynamic polarization plots of the Ti64 substrates were monitored from $-$ 0.250 *vs* OCP to 2 V *vs* SCE, with a scan rate of 0.1667 mV/s. Electrochemical impedance spectroscopic (EIS) data were monitored at the OCP by sweeping a frequency region from 10^5 to 10^{-2} Hz with a perturbation amplitude of 10 mV. Gamry Echem Analyst (version 7.05) was used to analyze the obtained EIS data through an equivalent circuit fitting procedure.

III. RESULT

A. Structure and Microstructure Analysis

The XRD patterns and microstructure analysis of the untreated and treated Ti64 groups are shown in Figures 1 and 2, respectively. The untreated alloy exhibited two phases ($\alpha + \beta$), a typical structure for the Ti64 alloy (Figure 1(a)). This structure is confirmed by the SEM images displayed in Figures 2(a) and (b), which showed a smooth flat surface consisting of α and β phases. The surface was not etched; therefore, the surface features and grains were not very clear. After
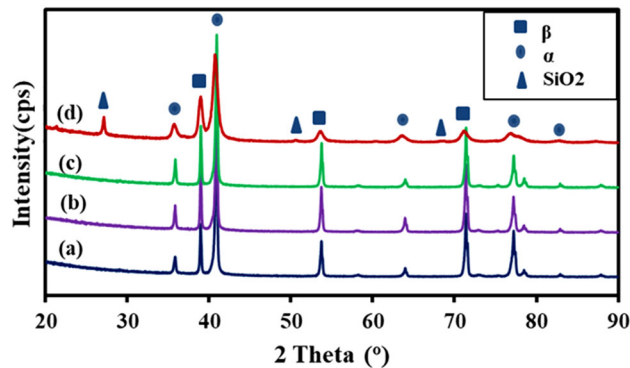
Fig. 1—XRD of Ti64 alloy: (*a*) untreated, (*b*) acid-treated (*c*) plasma-treated, (*d*) sandblasted.

CT and PT, XRD (Figures 1(c), (d) through (f)) showed neither a modification in the phases nor the appearance of any new phases. The microstructure of the chemically treated alloy sample (Figures 2(c) and (d)) represents an etched surface with a distinct β phase and α matrix. No change was observed in the phases of the alloy after plasma treatment, as observed in Figures 1(e) and (f); meanwhile, the SEM images showed a clear phase region with a grain boundary. The XRD pattern of the alloy surface treated with sandblasting indicated an (α + β) phase and SiO_2. A significant change occurred in the microstructure of SB, in which the smooth flat surface was transformed into coarse and rough morphologies consisting of pits and valleys, as shown in Figures 2(g) and (h), with an irregular sharp edge. This is typically due to the impingement of silica particles. It is also worth noting that chemical or plasma treatment did not produce any residual or oxidizing effects on the surface of the alloy. The elemental analysis of SB revealed the presence of Si and O due to residues of silica particles on the alloy surface used in the sandblasting process, as confirmed using XRD analysis. The distribution of silica particles is localized, as shown in the EDS mapping analysis (Figure 3). The XRD pattern shows a broadening of the peaks of the SB sample compared to the untreated samples, indicating a decrease in crystallite size (Figure 1).

B. Surface Roughness

The optical profilometer images of the untreated and treated Ti64 alloys are shown in Figure 4. The untreated and PT samples demonstrated a smooth surface, whereas the CT and SB samples had a rough surface. The surface roughness was quantified using the arithmetic average height (Ra). The untreated sample showed a microroughness of 0.17 μm, which slightly increased to 0.121 μm after CT. The PT smoothed the surface and resulted in an Ra value of 0.114 μm. However, SB increased the surface roughness by 10 times to 1.108 μm. However, the surface roughness on the nanoscale of the treated samples cannot be detected by an optical profilometer; therefore, AFM was used to measure the characteristics of the nanotextured surface. The topography and nanoscale surface roughness of the Ti64 alloy were characterized by AFM before and after surface treatment (Agilent 5500). The base alloy sample showed fine features with the lowest roughness parameters, as shown in Table I, and the samples after surface treatment generally exhibited improved alloy surface roughness. After chemical and plasma treatment, the alloy sample exhibited slightly increased surface roughness owing to the chemical and plasma etching effects. The similarity between the baseline, chemical, and plasma-treated topography, as shown in Figures 5(a) through (c), is due to the prior machining effect of the alloy. A significant change in topography with irregular features and roughness was observed in sandblasted samples due to the plastic deformation of the alloy surface during the sandblasting process, as shown in Figure 5(d). In Figure 5(d), the roughness profiles of the SB samples are shown; however, the untreated alloy profile was soft and uniform, whereas in the case of chemical and plasma-treated samples, the profile was brittle at some locations. In contrast, the sandblasted surface profile was jagged with large deflections due to the valleys formed in the sandblasting process.

C. Wetting Behavior

Wettability measurements were carried out to better understand the interaction between the treated surface and the physiological media. Wettability affects cell adhesion and protein absorption. The surface hydrophilicity was investigated by measuring the contact angle. A photograph of the water droplet along with the contact angle measured for both DI water and glycerol is shown in Figure 6 for the bare and different treated samples. The CA for the PT and SB samples was reduced compared to that of the untreated samples. The PT sample was influenced by the plasma bombardment, which resulted in the hydrophilicity of the surface. The CA of the bare sample was ~ 49.25 ± 1.13 and 66.72 ± 2.18 deg using water and glycerol, respectively. After sandblasting for 5 minutes, the CA decreased to 32.29 ± 3.28 deg with water and 57.03 ± 3.59 deg with glycerol. The reduction in the contact angle of SB is associated with an increase in the surface roughness of the SB sample, which leads to an increase in the surface area. The trend of the result agrees with a previous report,[24,25] which showed that the contact angle decreased as the titanium implant surface area increased. In contrast, the chemical treatment increased the CA to ~ 66.56 ± 4.98 and 69.38 ± 2.91 deg using water and glycerol, respectively. The plasma-treated samples had the most hydrophilic surface with CA of ~ 12.61 ± 3.49 and 27.17 ± 3.09 deg using water and glycerol, respectively.

D. In Vitro Corrosion Study in Artificial Saliva

The Nyquist plot in Figures 7(a) and (b), illustrates the progress of the monitored impedance as a function of the real and imaginary components. Portions of the plots were enlarged to visualize the investigated substrates because of the variance of scale in Z_{real} and $Z_{imaginary}$. The Nyquist plots of the bare substrate
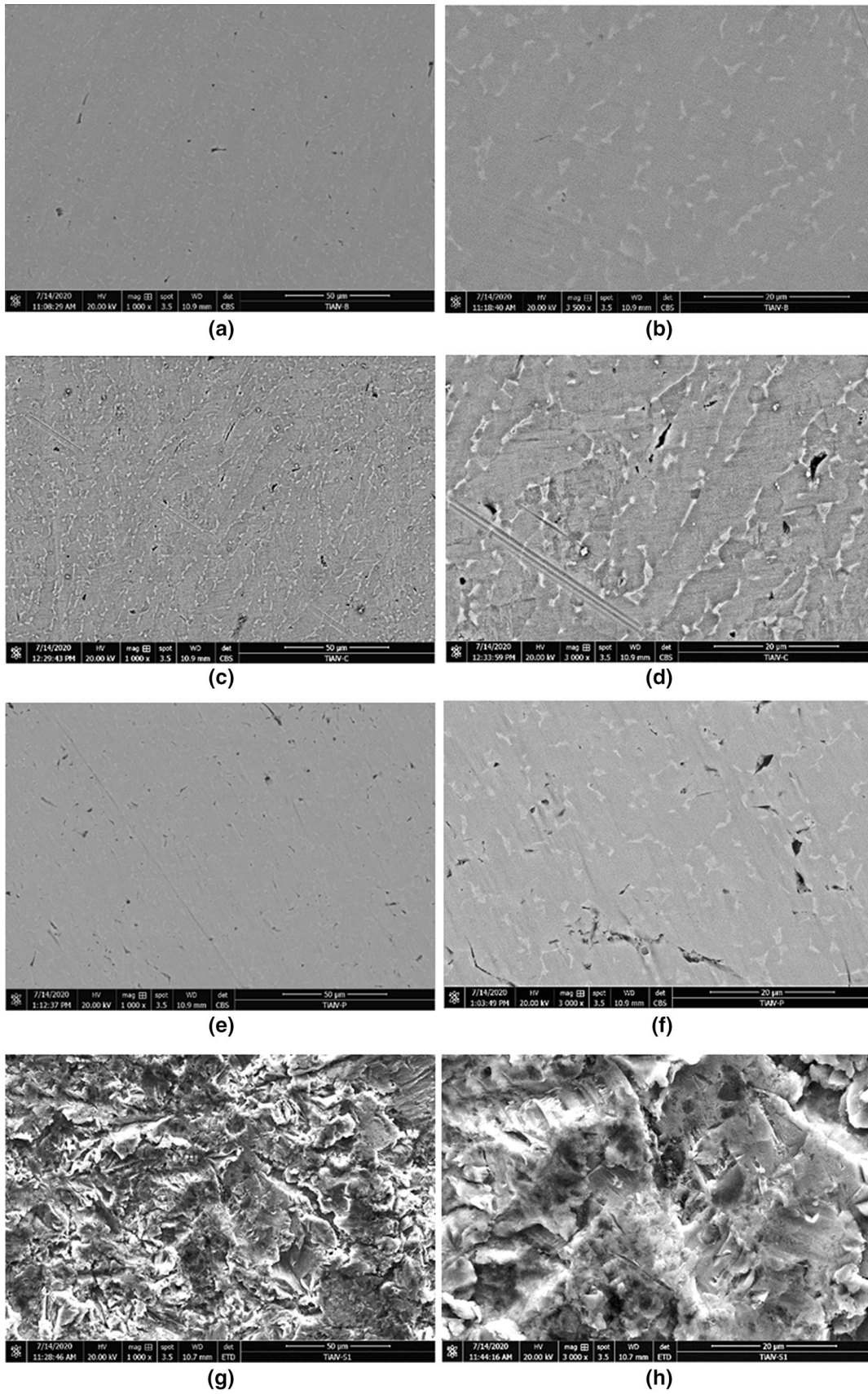
Fig. 2—SEM of (*a*, *b*) untreated Ti64 alloy, (*c*, *d*) acid-treated, (*e*, *f*) plasma-treated, (*g*, *h*) sandblasted.
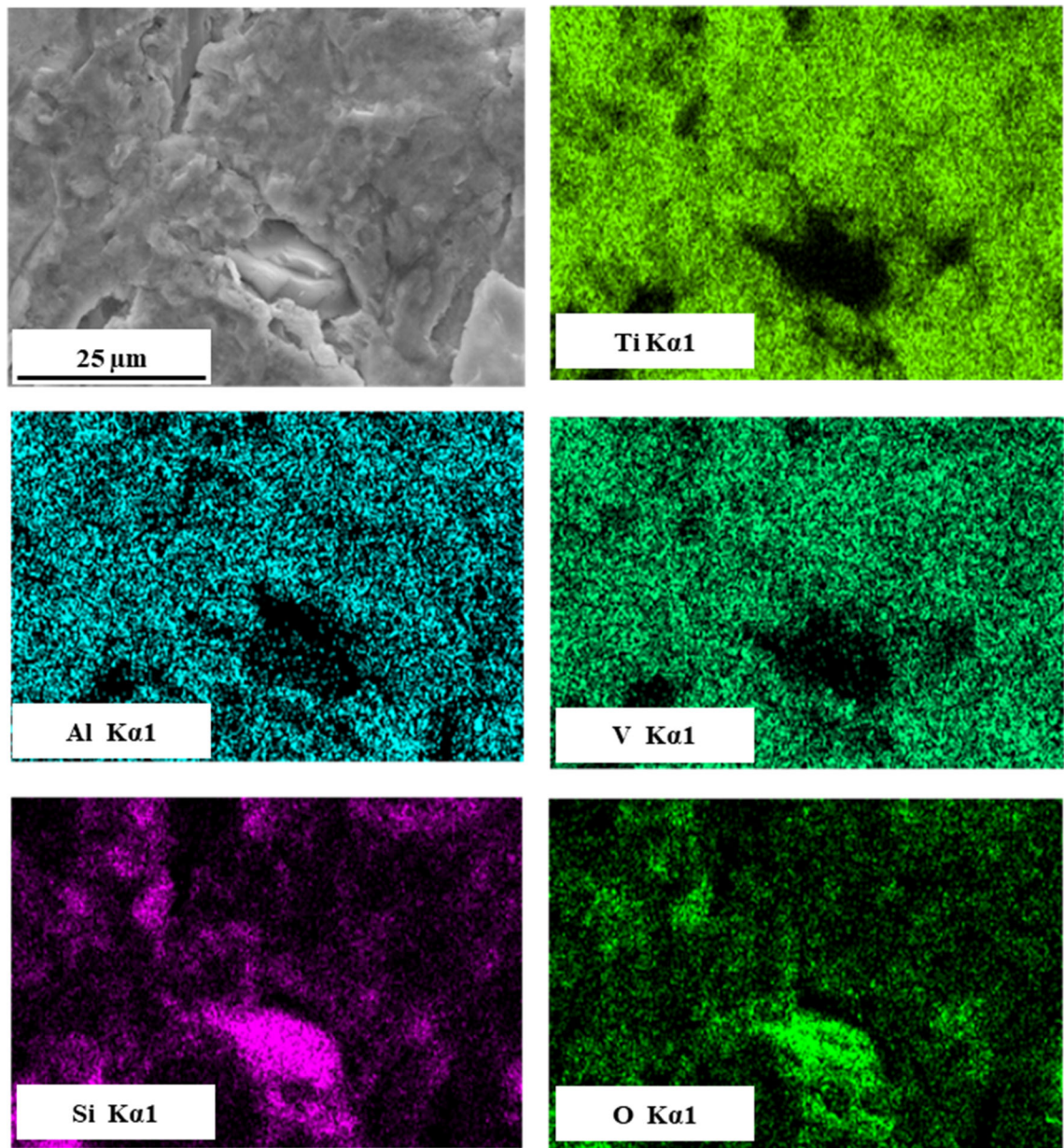
Fig. 3—EDS mapping of elements in sandblasted Ti64 alloy.

displayed a capacitive loop, while the treated substrates exhibited a capacitive arc with linear-like behavior in both electrolytes. Bode plots (Figures 8(a) and (b)) show the difference in the observed impedance as a function of the frequency of the electrochemical double layer produced at the interface of Ti during corrosion reactions. It can be observed that all Bode plots display two distinct regions, with the higher frequency region revealing a constant $|Z|$ value and a lower phase angle, attributed to solution resistance.[26,27] As the frequency decreases, $|Z|$ gradually increases with an increase in the phase angle and shows a united slope at approximately -1, demonstrating a characteristic response of capacitive performance.[28]

To quantitatively evaluate the electrochemical corrosion behavior of bare and surface-treated substrates, EIS circuit fitting analyses were performed by selecting the proper equivalent circuit (EC) model. Following the observed quarter capacitive arc and only one time constant in the EIS plots, the adapted Randle's circuit $[R_s (R_{ct}CPE_{dl})]$ (Figure 9) was utilized to fit the obtained EIS data.[29,30] This EIS circuit model was comprised of a parallel combination in series with the electrolytic resistance (R_s) between the working and reference electrodes. A constant phase element (CPE) was engaged on behalf of the capacitor, compensating for the non-ideal performance owing to the effect of dissimilarities from the surface heterogeneities of the
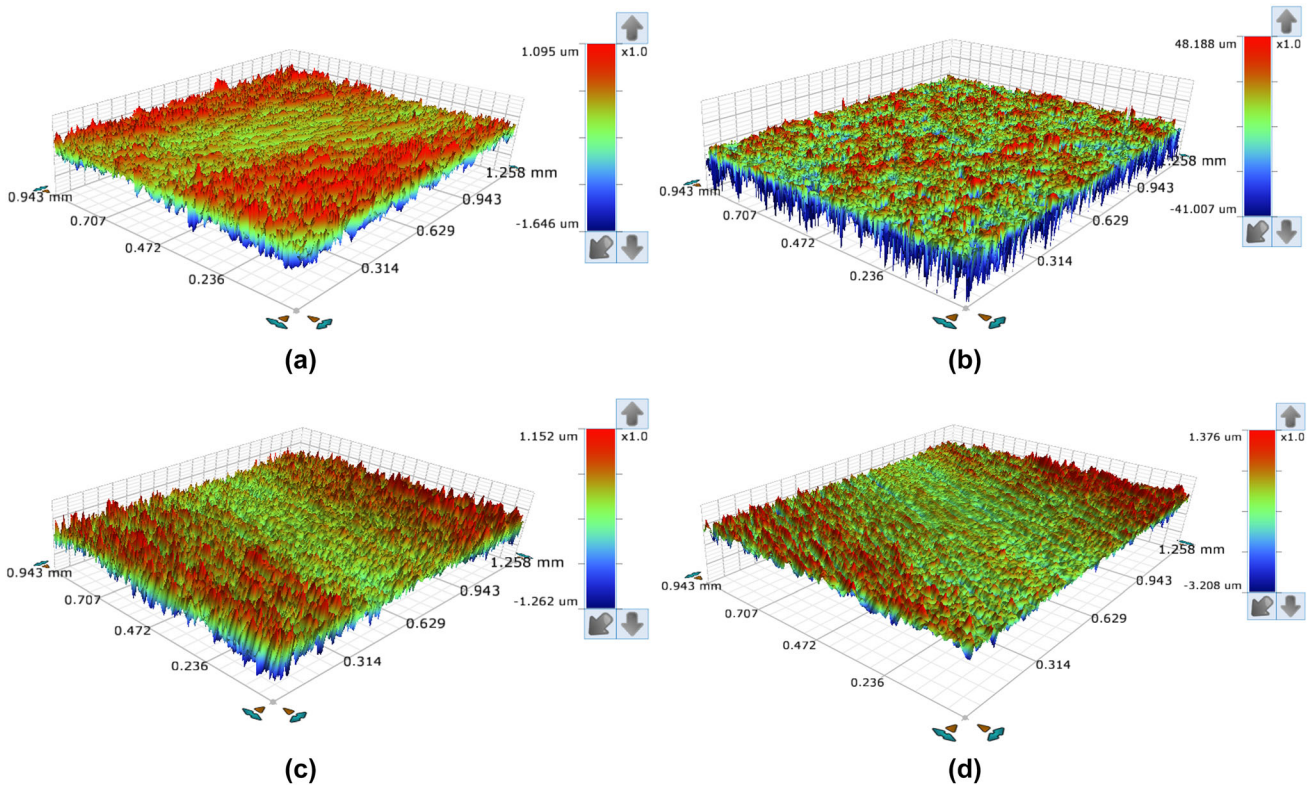
Fig. 4—Three-dimensional surface topography for (*a*) bare Ti64 sample, (*b*) sandblasted (*c*) chemical-treated, (*d*) plasma-treated.

Table I. Surface Roughness of Untreated and Treated Ti64 Alloy

Sample	Ra (μm) Microscale	Ra (nm) Nanoscale
Untreated	0.117	6.1
Chemically Treated	0.121	13.3
Plasma-Treated	0.114	8.52
Sandblasted	1.108	48.9

substrates. All the investigated substrates provided a goodness of fit below 10^{-4}, indicating a satisfactory quality of fitting for the selected EC model.

The typical PDP curves of the bare and surface-treated Ti64 substrates in AS medium with and without fluoride are presented in Figure 10. The cathodic polarization curves of all the investigated substrates exhibited almost similar trends in AS with and without fluoride. However, the anodic curves exhibit significant changes in their potential domains with passivation characteristics. Bare Ti64 substrates showed a sharp anodic slope from − 255 to 250 mV, indicating anodic dissolution. This remained almost vertical with a smaller slope, which was constant, up to 1500 mV before anodic dissolution gradually occurred up to 2000 mV. In contrast, the plasma-treated and chemically treated substrates displayed different trends in comparison with the bare and sandblasted substrates. The anodic slope was found to be less vertical, signifying

reduced dissolution. Furthermore, unlike the bare substrate, the plasma and chemically treated substrates exhibited a reduced current density in the section ranging from the initiation of anodic polarization to approximately 1000 mV and remained constant up to 2000 mV. The electrochemical parameters obtained from the Tafel analysis are listed in Table II. The corrosion current densities (i_{corr}) of the surface-treated substrates were found to be lower than those of the bare substrates in both electrolytes. In addition, the passive current density (i_{p}) values of the surface-treated substrates were lower than that of the bare substrate (~ 85 μA cm^{-2}).

IV. DISCUSSION

The implant surface has a significant effect on its interaction with surrounding tissues *in vivo* and on its functional lifespan. Surface features, including composition, microtopography, roughness, and surface energy, influence the adherence and distribution of bone precursor cells, as well as their future proliferation and differentiation.[31,32] In the present study, we investigated biomedical Ti64 alloys with different surface modifications: plasma treatment, sandblasting, and acid treatment. The surface characteristics obtained through surface modifications may indicate that the treated Ti6Al4V alloy had improved surface and *in vitro* corrosion properties in artificial saliva, making it a potential candidate for dental applications.
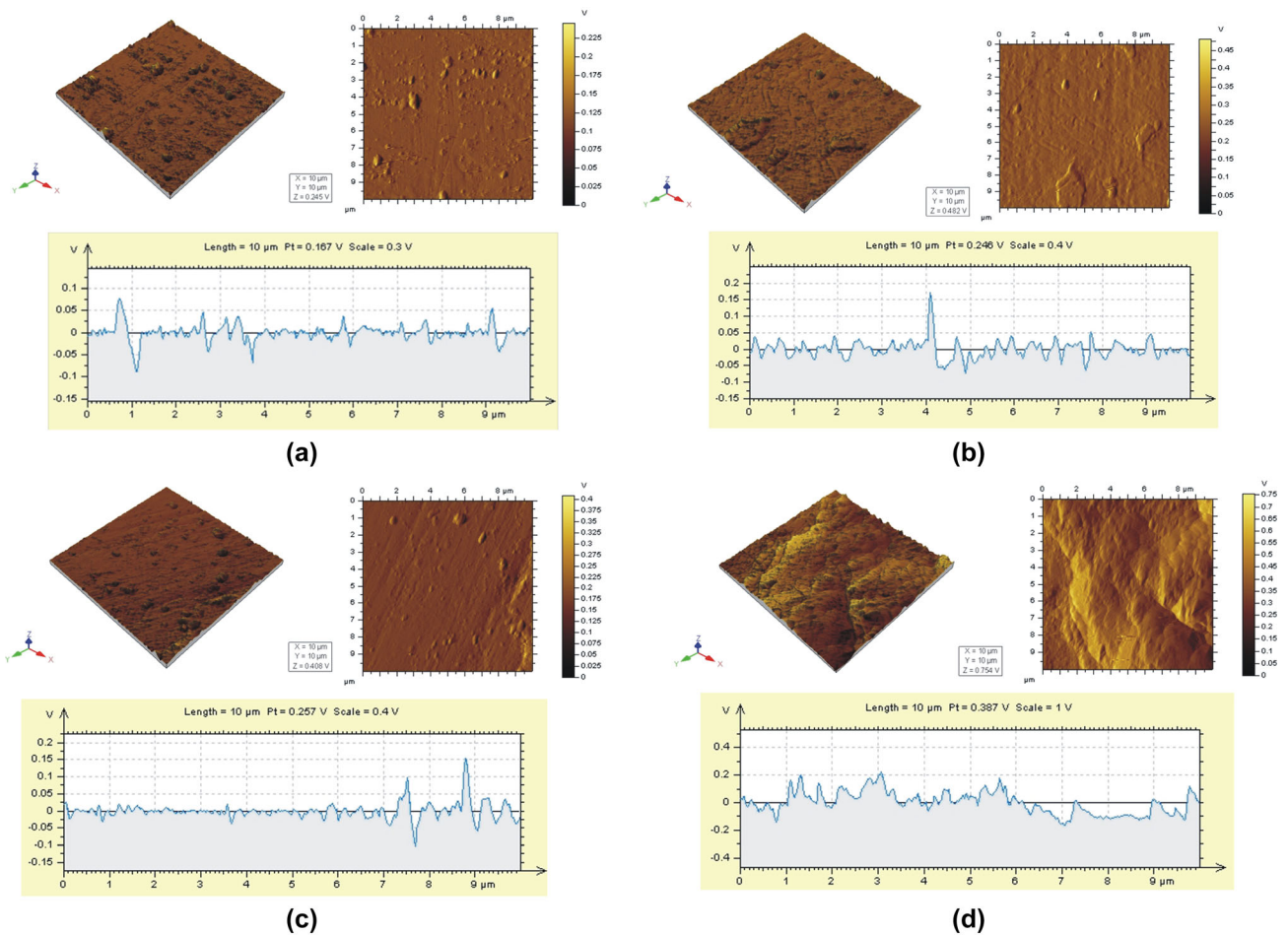
Fig. 5—AFM morphologies and roughness profiles of Ti64 surfaces: (*a*) bare sample, (*b*) chemical-treated, (*c*) plasma-treated and (*d*) sandblasted.

Structural and microstructural investigations revealed that the untreated and treated alloys exhibited two phases ($\alpha + \beta$). A matrix of the α phase, along with the β phase, is impeded in the α matrix, and no evidence of the occurrence of secondary phases was observed. Etching creates an irregular surface. A flake-like microstructure was observed in the flat region. The crystallite sizes of the untreated and treated samples were calculated according to the Scherrer equation.[1] The crystallite size of SB samples (Figure 1(d)) was decreased to 10.8 nm compared to 41.9 nm for the untreated sample, which is in agreement with the previous finding.[33] However, the PT (48.5 nm) and CT (44.6 nm) samples showed an almost negligible change in the crystallite size compared to the untreated sample.

The surface roughness of potential implant materials is crucial for bone growth at the bone-implant interface.[34] The functional activity of cells interacting with biomaterials is influenced by surface features. To investigate the effect of surface modifications on the surface roughness, topography, microscale, and nanoscale surface roughness of untreated and treated Ti64 alloys were characterized using surface profilometry and AFM, respectively. The sandblasting treatment produced a relatively high roughness owing to the impact of sand

particles on the surface. The microscale surface roughness showed that the treatment of plasma and chemical mixtures had a negligible effect on the surface roughness. However, the nanoscale roughness showed that following chemical and plasma treatment, the surface roughness of the alloy sample increased marginally as a result of the chemical and plasma etching effects. In sandblasted samples, a considerable change in topography with irregular features and roughness was found as a result of the plastic deformation of the alloy surface during the sandblasting process. Among the treated samples, the SB samples exhibited the highest surface roughness. Rough-textured biomaterial surfaces are believed to improve osteoblast cell attachment and osteoblast formation.[35–37] The increased surface roughness increases the grain boundary per unit area and enables cell adhesion on the surface.[38] It has been reported that roughness and alloy properties are both important for cell activity.[39,40] The cell adhesion was dependent on the thickness of the titanium oxide, as well as the microporosity and roughness of the surface.[41]

Surface hydrophilicity impacts cell adhesion proteins and enhances adhesion. Among the surface-treated samples, CT and PT increased the wettability of the surface due to the higher surface area exposure, increase
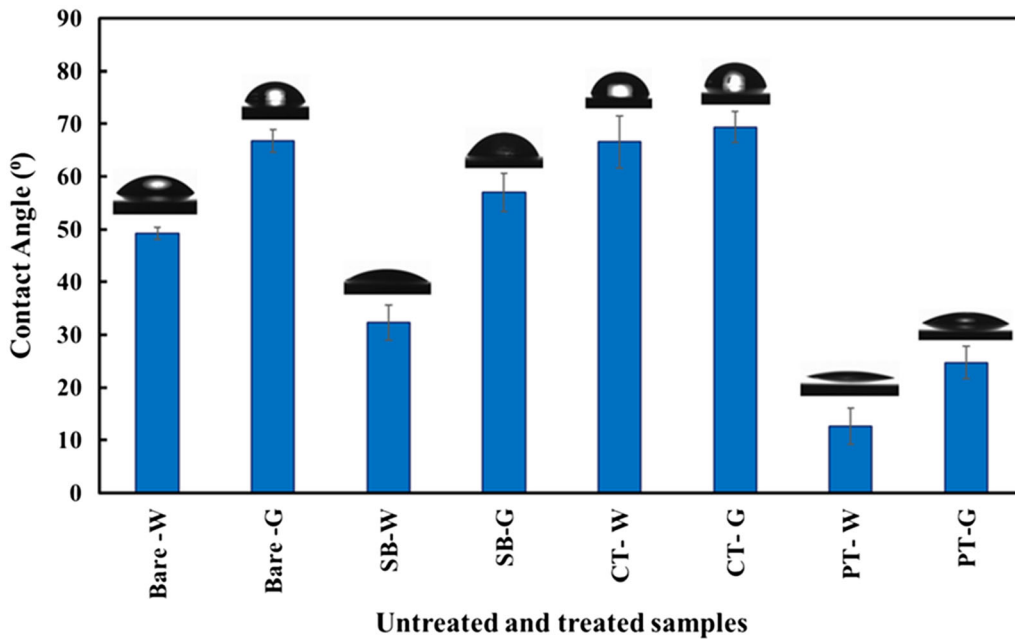
Fig. 6—Water (W) and glycerol (G) contact angle for untreated and treated Ti64 samples.
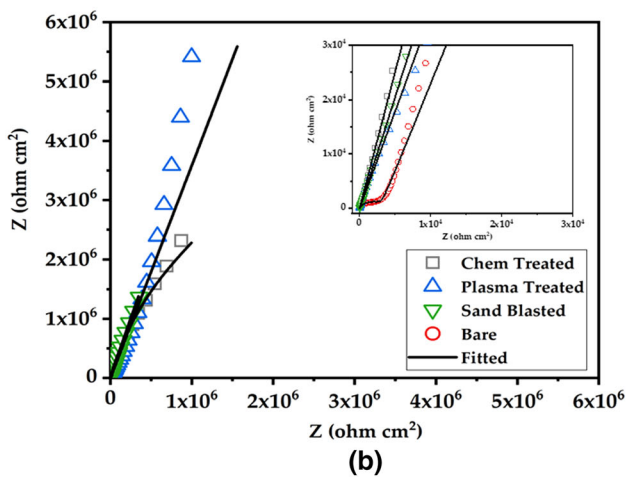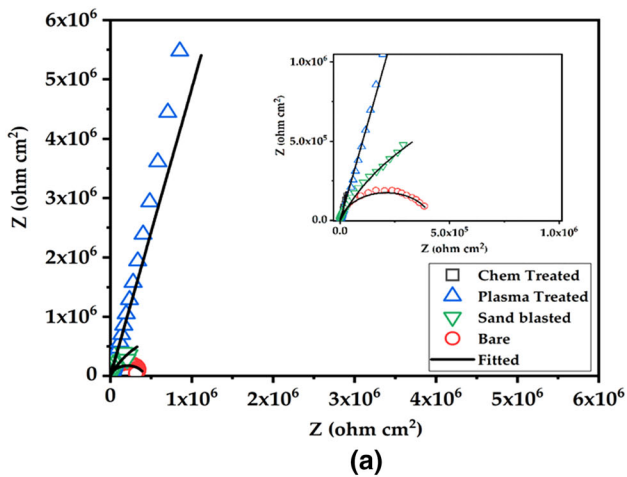

Fig. 7—Nyquist plots of surface-treated substrates in (a) AS medium, (b) AS medium with fluorides.

in surface roughness, and removal of the oxide layer. The results showed that sandblasting treatment and plasma treatment reduced the water contact angle to 32.2 and 12.61 deg, respectively, indicating the attainment of a hydrophilic surface with surface modifications. The XRD pattern (Figures 1(c) and (d)) of the SB sample showed a higher full width at half maximum (FWHM) than the untreated samples, which indicated a decrease in the crystallite size (10.8 nm) compared to 41.9 nm for the untreated sample. Therefore, the wettability result showed a decrease in the contact angle with the decrease in crystallite size, which agrees with a previous report.[33] Surface energy significantly affects intermolecular interactions, surface wetting, and adsorption behavior with other materials. The surface energies of the untreated and treated samples were calculated using contact angle measurements of water and glycerol according to Owens-Wendt.[14,22,23] Table III presents the contact angle, polar and dispersive components, and total surface energy values. The samples showed a surface energy range of 36.88 to 67.196 mJ/m^2. SB and PT improved the hydrophilicity of the surface by increasing the contact angle and decreasing the surface energy. Surface wetness has a significant influence on the initial attachment and proliferation of cells.[42] Surface wettability affects surface energy. Increasing the surface energy enhances the interaction of liquids and proteins with titanium [43] according to the Wenzel formula, and hydrophilic surface roughness promotes wetting.

The observed semicircular arc in the Nyquist plots revealed that the treated surfaces interfere with the charge transfer reactions at the metal/electrolyte interface. It is obvious that the different quarter-arcs shown in the Nyquist graphs of Figure 7 and their radii indicate the corrosion resistance.[26] The bare substrates
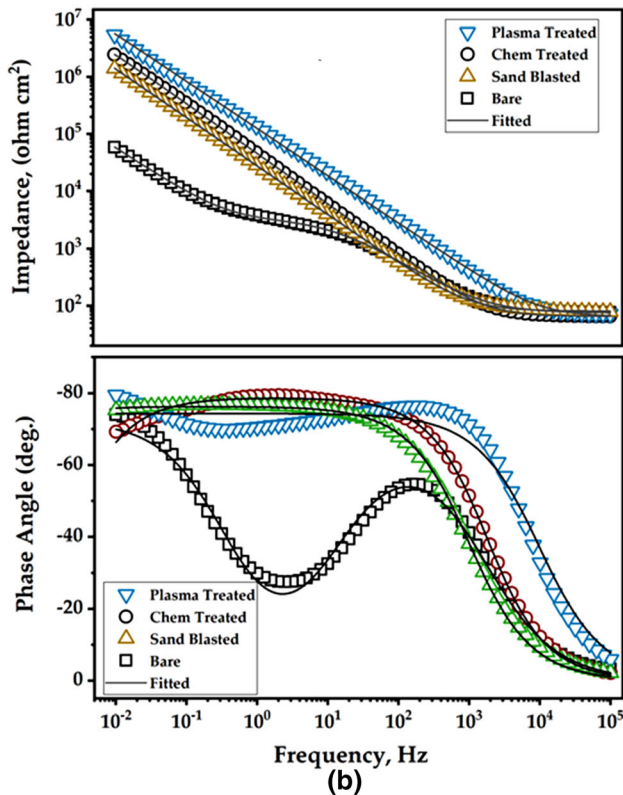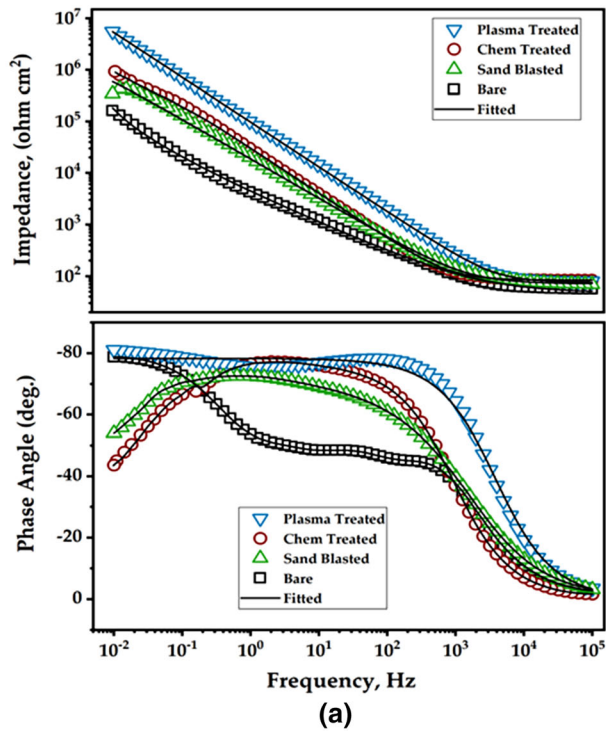
Fig. 9—EIS circuit model of modified Randles model.
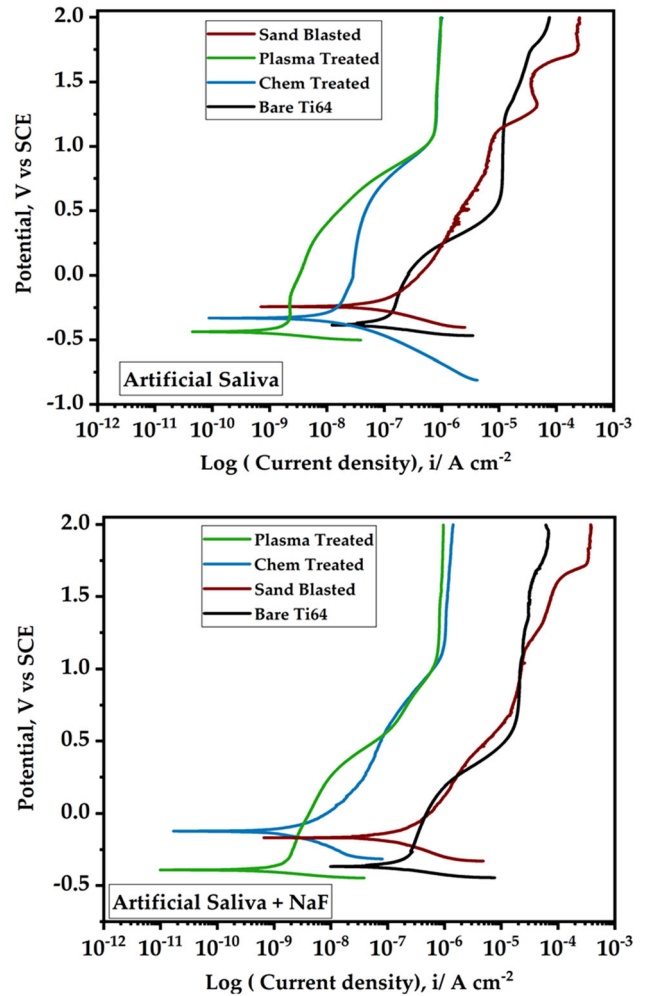
Fig. 10—PDP curves of surface-treated substrates in AS medium with and without fluorides.

Fig. 8—Bode plots of surface-treated substrates in (*a*) AS medium (*b*) AS medium with fluorides.

exposed to AS with NaF exhibited a reduction in the semicircular radii of the capacitive arc, which indicates lower corrosion resistance. However, the treated substrates showed improved corrosion resistance in the AS
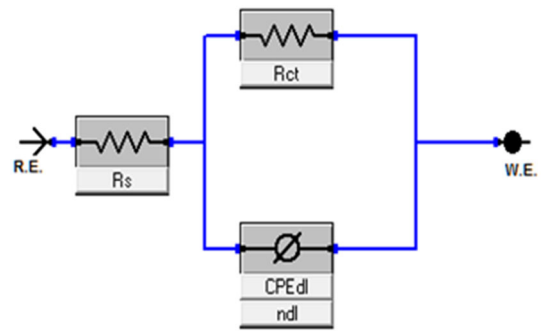
medium with NaF. The impedance modulus |*Z*| at 0.01 Hz signifies the polarization resistances of the substrate, which is evidently higher for the surface-treated substrates, signifying a higher corrosion resistance performance. The phase angle for the bare substrate in AS with NaF showed the lowest angle that validated the poorest corrosion resistance of bare substrate due to aggressive fluoride ions, which accelerated the corrosion rate of bare substrates by destroying the protective

Table II. Electrochemical Corrosion Parameters for the Surface-Treated Substrates in AS Medium With and Without Fluorides

Medium	Samples	E_{corr} V	i_{corr} A cm^2 x 10^{-7}	i_p A cm^2 x 10^{-7}	R_s Ω cm^2	R_{ct} kΩ cm^2	CPE$_{dl}$ μF cm^{-2}	n_{dl}
AS	Untreated Surface	− 0.414	1.128	115.047	74.59	168541	10.251	0.95
	SB	− 0.231	0.789	31.97	69.25	361893	0.182	0.96
	CT	− 0.318	0.126	8.125	71.22	897927	0.094	0.98
	PT	− 0.407	0.091	6.125	65.58	5800848	0.017	0.98
AS + NaF	Untreated Surface	− 0.351	2.178	289.217	84.57	57980	28.540	0.94
	SB	− 0.162	1.228	209.641	78.28	1311246	1.947	0.95
	CT	− 0.116	0.047	10.087	81.24	2504548	1.054	0.97
	PT	− 0.372	0.011	7.821	83.98	6004001	0.098	0.97

Table III. Contact Angle and Surface Energy for Untreated and Treated Ti64 Samples

Sample	Water Contact Angle (°)	Glycerol Contact Angle (°)	γ_s^d (mJ/m^2)	γ_s^p (mJ/m^2)	γ_s (mJ/m^2)
Untreated Surface	49.25	66.72	0.120	67.07	67.196
CT	66.56	69.38	5.276	31.606	36.88
PT	12.61	24.71	10.30	63.52	73.82
SB	32.29	57.03	0.0519	85.67	85.72

passive layer. In general, the value of R_{ct} is the resistance of the charge transfer through the passive layer and is directly governed by the rate of anodic dissolution, and a higher R_{ct} indicates improved corrosion resistance performance.[44] As shown in Table II, the R_{ct} values of the plasma-treated and chemically treated substrates were higher than those of the other substrates, revealing that the corrosion process was effectively suppressed at the metal/electrolyte interface. In addition, the lowest constant phase element of the double layer capacitance (CPE$_{dl}$) value of these substrates validates the reduced dissolution and improved passivation behavior. The maximum n$_{dl}$ value of these substrates also validated the homogeneity of the passive layer formed on its surface, which confirmed the enhanced corrosion-resistant behavior in the AS medium.

The shape of the obtained cathodic branches in the PDP curves (Figure 10) suggested that the cathodic reactions occurring in both solutions are almost similar at different rates. However, the anodic behavior of the treated surfaces can be ascribed to the low diffusion of oxygen because of the existence of a passive film on the Ti substrate. In comparison with the bare samples, the sandblasted substrates exhibited almost similar behavior with some fluctuation in the anodic region due to the presence of an active surface with high surface roughness produced during this treatment. Hence, the obtained results reveal that the plasma-treated and chemically treated substrates showed a passive state in AS with and without fluorides, while the bare and sandblasted substrates exhibited active behavior. In particular, the plasma-treated and chemically treated substrates displayed a positive transpassive dissolution potential and wider passive region than the bare and

sandblasted substrates in both electrolytes. This indicates that the passivation film of the plasma-treated and chemically treated substrate exhibited better corrosion resistance behavior than that of the bare and sandblasted substrates. From the obtained EIS and PDP results, it was concluded that bare and sandblasted samples exhibited the lowest corrosion resistance in the AS medium with and without fluorides, with the lowest R_{ct} and highest CPE$_{dl}$ and i_{corr} values. Meanwhile, plasma and chemically treated substrates showed an improved corrosion resistance behavior in AS medium with and without fluorides, displaying higher R_{ct} and the lowest CPE$_{dl}$ and i_{corr} values. Thus, the corrosion resistance performance of the treated substrates increased in the following order: bare < sandblasted < chemically treated < plasma-treated.

V. CONCLUSIONS

Surface analysis and *in vitro* corrosion studies were performed in artificial saliva for three different surface treatments performed on Ti64 alloy: chemical treatment, plasma treatment, and sandblasting. Several analytical tools were used for the physicochemical analysis of untreated and treated surfaces, such as AFM, surface profilometry, contact angle measurements, SEM/EDS, and XRD. Electrochemical analysis was performed using PDP and EIS in artificial saliva to assess the corrosion performance of the treated surfaces, and the following conclusions were drawn:

1. Sandblasting decreases the crystallite size of the alloy surface to 10.8 nm.

2. The water contact angles decreased to 15 and 35 deg after plasma treatment and sandblasting, respectively.
3. The surface energy increased by 10 and 28 pct after plasma treatment and sandblasting, respectively.
4. The obtained in vitro corrosion test results validated that the plasma-treated surface exhibited the highest charge transfer resistance (R_{ct}) and lowest capacitance and corrosion current density (i_{corr}) values, indicating its beneficial role in improving the corrosion resistance of Ti64 alloy substrates.
5. Fluoride addition slightly reduced the corrosion resistance of all the investigated-treated surfaces.
6. With the limitation of the current study, the results indicate that the treated Ti6Al4V alloy showed enhanced surface and *in vitro* corrosion protection, making it a candidate for dental applications.

ACKNOWLEDGMENTS

CONFLICT OF INTEREST

The authors declare that there is no conflict of interest.

REFERENCES

1. M.A. Hussein, N.K. Ankah, A. Madhan Kumar, M.A. Azeem, S. Saravanan, A.A. Sorour, and N. Aqeeli: *Ceram. Int.*, 2020, vol. 46, pp. 18573–83.
2. M.A. Hussein, C. Suryanarayana, and N. Al-Aqeeli: *Mater. Des.*, 2015, vol. 87, pp. 693–700.
3. F. Melo-Fonseca, M. Gasik, S. Madeira, F.S. Silva, and G. Miranda: *Mater. Charact.*, 2021, vol. 177, art. no. 111161.
4. M.A. Hussein, A. Madhan Kumar, N. Ankah, and M. A. Azeem: *Ceram. Int.*, 2021.
5. N. Sirdeshmukh and G. Dongre: *Mater. Today*, 2021, vol. 44, pp. 2348–55.
6. Y. Yan, E. Chibowski, and A. Szcześ: *Mater. Sci. Eng. C.*, 2017, vol. 70, pp. 207–15.
7. A. Noro, M. Kaneko, I. Murata, and M. Yoshinari: *J. Biomed. Mater. Res. B*, 2013, vol. 101, pp. 355–63.
8. A. Jemat, M.J. Ghazali, M. Razali, and Y. Otsuka: *Biomed. Res. Int.*, 2015, vol. 2015, pp. 1–11.
9. S. Wang, W. Dongle, H. She, W. Mingxu, D. Shu, A. Dong, H. Lai, and B. Sun: *Mater. Sci. Eng. C*, 2020, vol. 113, art. no. 110959.
10. C. Nune, R.D.K. Misra, M.C. Somani, and L.P. Karjalainen: *J. Biomed. Mater. Res. A*, 2014, vol. 102, pp. 1663–76.
11. A. Madhan Kumar, M.A. Hussein, A.Y. Adesina, S. Ramakrishna, and N. Al-Aqeeli: *RSC advances*, 2018, vol. 8, pp. 19181–95.
12. V.K. Truong, R. Lapovok, Y.S. Estrin, S. Rundell, J.Y. Wang, C.J. Fluke, R.J. Crawford, and E.P. Ivanova: *Biomaterials*, 2010, vol. 31, pp. 3674–83.
13. R.Z. Valiev, I.P. Semenova, V.V. Latysh, H. Rack, T.C. Lowe, J. Petruzelka, L. Dluhos, D. Hrusak, and J. Sochova: *Adv. Eng. Mater.*, 2008, vol. 10, pp. 15–17.
14. M.A. Hussein, B. Yilbas, A. Madhan Kumar, R. Drew, and N. Al-Aqeeli: *J. Mater. Eng. Perform.*, 2018, vol. 9, pp. 4655–64.
15. I. Shivakoti, G. Kibria, S. Das, A. Sharma, B.B. Pradhan, and S. Chatterjee: *Mater. Manuf. Process.*, 2021, vol. 36, pp. 858–67.
16. M. Arregui, F. Latour, F.J. Gil, R.A. Pérez, L. Giner-Tarrida, and L.M. Delgado: *Coatings*, 2021, vol. 11, p. 98.
17. E.J. Kassab, C.D. dos Reis Barros, P.G. Silva, L.F. Silva, and J.A.P. Gomes: *J. Mater. Eng. Perform.*, 2021, vol. 30, pp. 994–1000.
18. E. Arslan, Y. Totik, E. Demirci, and A. Alsaran: *J. Mater. Eng. Perform.*, 2010, vol. 19, pp. 428–33.
19. C. Vitelaru, N. Ghiban, A.C. Parau, M. Balaceanu, F. Miculescu, and A. Vladescu: *Materialwiss Werkst*, 2014, vol. 45, pp. 91–98.
20. J. Fojt, V. Hybášek, Z. Kačenka, and E. Průchová: *Metals*, 2020, vol. 10, p. 1547.
21. G. Wang, Y. Wan, T. Wang, and Z. Liu: *Procedia Manuf*, 2017, vol. 10, pp. 363–70.
22. T. Senturk Parreidt, M. Schmid, and C. Hauser: *Foods*, 2017, vol. 6, p. 31.
23. Z. Zhong, S. Yin, C. Liu, Y. Zhong, W. Zhang, D. Shi, and C. Wang: *Appl. Surf. Sci.*, 2003, vol. 207, pp. 183–89.
24. R.V. Bathomarco, G. Solorzano, C.N. Elias, and R. Prioli: *Appl. Surf. Sci.*, 2004, vol. 233, pp. 29–34.
25. C.N. Elias, Y. Oshida, J.H.C. Lima, and C.A. Muller: *J. Mech. Behav. Biomed. Mater.*, 2008, vol. 1, pp. 234–42.
26. M.A. Hussein, M. Kumar, R. Drew, and N. Al-Aqeeli: *Materials*, 2018, vol. 11, pp. 1–15.
27. A Madhan Kumar, MA Hussein, AY Adesina, and N Al-Aqeeli: *Coatings*, 2019, vol. 9, p. 344.
28. A. Madhan Kumar, P. Sudhagar, S. Ramakrishna, Y.S. Kang, H. Kim, Z.M. Gasem, and N. Rajendran: *Appl. Surf. Sci.*, 2014, vol. 307, pp. 52–61.
29. Y.-y. Guo, M.-q. Cheng, D.-s. Chen, X.-b. Xue, and X.-l. Zhang: *Trans. Nonferrous Met. Soc. China*, 2012, vol. 22, pp. 175–80.
30. A.K. Shukla and R. Balasubramaniam: *Corros. Sci.*, 2006, vol. 48, pp. 1696–1720.
31. S. Asadullah, S. Mei, D. Wang, Y. Yao, Y. Pan, D. Wang, H. Guo, and J. Wei: *Mater. Des.*, 2020, vol. 190, p. 108510.
32. F. Rupp, L. Liang, J. Geis-Gerstorfer, L. Scheideler, and F. Hüttig: *Dent. Mater.*, 2018, vol. 34, pp. 40–57.
33. A. Günay-Bulutsuz, Ö. Berrak, H. AygülYeprem, E.D. Arisan, and M.E. Yurci: *Mater. Sci. Eng. C*, 2018, vol. 91, pp. 382–88.
34. A. Agno and D.D. Bello: *J. Mater. Sci. Mater. Med.*, 2004, vol. 15, pp. 935–49.
35. F. Lüthen, R. Lange, P. Becker, J. Rychly, U. Beck, and J.G. BarbaraNebe: *Biomaterials*, 2005, vol. 26, pp. 2423–40.
36. S. Ponader, E. Vairaktaris, P. Heinl, C.V. Wilmowsky, A. Rottmair *et al.*: *J. Biomed. Mater. Res. A.*, 2008, vol. 84, pp. 1111–19.
37. D.D. Deligianni, N. Katsala, S. Ladas, D. Sotiropoulou, J. Amedee, and Y.F. Missirlis: *Biomaterials*, 2001, vol. 22, pp. 1241–51.
38. Y. Geng, É. McCarthy, D. Brabazon, and N. Harrison: *Surf. Coat. Technol.*, 2020, vol. 398, p. 126085.
39. C. Eriksson, J. Lausmaa, and H. Nygren: *Biomaterials*, 2001, vol. 22, pp. 1987–96.
40. J.Y. Martin, Z. Schwartz, T.W. Hummert, D.M. Schraub, J. Simpson, J. Lankford, D.D. Dean, D.L. Cochran, and B.D. Boyan: *J. Biomed. Mater. Res.*, 1995, vol. 29, pp. 389–401.
41. X.L. Zhu, J. Chen, L. Scheideler, R. Reichl, and J. Geis-Gerstorfer: *Biomaterials*, 2004, vol. 25, pp. 4087–4103.
42. L. Le Guéhennec, A. Soueidan, P. Layrolle, and Y. Amouriq: *Dent. Mater.*, 2007, vol. 23, pp. 844–54.
43. M.H. Zhao, X.P. Chen, and Q. Wang: *Sci. Rep.*, 2014, vol. 4, pp. 1–5.
44. X. He, G. Zhang, X. Wang, R. Hang, X. Huang, L. Qin, B. Tang, and X. Zhang: *Ceram. Int.*, 2017, vol. 43, pp. 16185–95.